Available online at www.sciencedirect.com
SCIENCE DIRECT®
Journal of Inorganic Biochemistry 93 (2003) 41–51
Journal of Inorganic Biochemistry
www.elsevier.com/locate/jinorgbio

Refinement of the nickel site structure in *Desulfovibrio gigas* hydrogenase using range-extended EXAFS spectroscopy

Weiwei Gu[a,b], L. Jacquamet[a], D.S. Patil[b], H-X. Wang[a], D.J. Evans[c], M.C. Smith[c], M. Millar[d], S. Koch[d], D.M. Eichhorn[e], M. Latimer[f], S.P. Cramer[a,b,*]

[a]*Department of Applied Science, University of California, 1 Shields Ave., Davis, CA 95616, USA*
[b]*Lawrence Berkeley National Laboratory, Berkeley, CA 94720, USA*
[c]*Department of Biological Chemistry, John Innes Centre, Norwich NR4 7UH, UK*
[d]*Department of Chemistry, State University of New York, Stony Brook, NY 11794, USA*
[e]*Department of Chemistry, Wichita State University, Wichita, KS 67260, USA*
[f]*Stanford Synchrotron Radiation Laboratory, Stanford, CA 94025, USA*

Received 2 January 2002; received in revised form 22 February 2002; accepted 19 March 2002

Abstract

We have reexamined the Ni EXAFS of oxidized, inactive (as-isolated) and H_2 reduced *Desulfovibrio gigas* hydrogenase. Better spatial resolution was achieved by analyzing the data over a 50% wider *k*-range than was previously available. A lower k_{min} was obtained using the FEFF code for phase shifts and amplitudes. A higher k_{max} was obtained by removing an interfering Cu signal from the raw spectra using multiple energy fluorescence detection. The larger *k*-range allowed us to better resolve the Ni–S bond lengths and to define more accurately the Ni–O and Ni–Fe bond lengths. We find that as-isolated, hydrogenase has two Ni–S bonds at ~2.2 Å, but also 1–2 Ni–S bonds in the 2.35±0.05 Å range. A Ni–O interaction is evident at 1.91 Å. The as-isolated Ni–Fe distance cannot be unambiguously determined. Upon H_2 reduction, two short Ni–S bonds persist at ~2.2 Å, but the remaining Ni–S bonds lengthen to 2.47±0.05 Å. Good simulations are obtained with a Ni–Fe distance at 2.52 Å, in agreement with crystal structures of the reduced enzyme. Although not evident in the crystal structures, an improvement in the fit is obtained by inclusion of one Ni–O interaction at 2.03 Å. Implications of these distances for the spin-state of H_2 reduced H_2ase are discussed.

Keywords: Hydrogenase; EXAFS; Ni enzymes; Synchrotron radiation

1. Introduction

The reversible oxidation of hydrogen to proton and electrons is one of the simplest reactions in nature, yet it has immense economic [1] and ecological importance [2]. At least 1.3% of U.S. primary energy production is converted to hydrogen for industrial chemical use [3], especially in refineries and ammonia plants. Increased use of hydrogen is expected as one approach to reducing CO_2 emissions and associated global warming effects [4].

In living organisms, the uptake and evolution of hydrogen is accomplished by the enzyme hydrogenase [5]. The *Desulfovibrio gigas* hydrogenase catalyzes the reversible oxidation of molecular hydrogen at an unusual Ni–Fe cluster [6]. The crystal structures for the inactive as-isolated enzyme reveal a Ni ligated by two terminal cysteine sulfurs, as well as two cysteine sulfurs that bridge to an $Fe(CO)(CN)_2$ unit [7]. An additional light atom, proposed to be an oxo or hydroxo bridge, completes the connection between Ni and Fe that are separated by ~2.9 Å. In the structures of *Desulfovibrio vulgaris* Miyazaki and *Desulfovibrio desulfuricans* ATCC 27774 hydrogenases, which are primarily in the 'ready' or form B state, a sulfur is proposed to occupy this site [8,9]. The light atom appears absent in crystal structures of the reduced and active forms of related hydrogenases, and the Ni–Fe distance contracts to ~2.5 Å [10,11]. The active site has been studied extensively by FT-IR [12–14], EPR [15–17], and EXAFS (Extended X-ray Absorption Fine Structure) [18–23] spectroscopies, as well as by density functional theory (DFT) calculations [24,25].

A precise understanding of the interatomic distances at the Ni–Fe center is important for an understanding of the

*Corresponding author. Fax: +1-510-486-5664.
E-mail address: spcramer@ucdavis.edu (S.P. Cramer).

0162-0134/02/$ – see front matter
PII: S0162-0134(02)00494-4

catalytic mechanism. The Ni–S bond lengths have implications for the protonation state of the thiolate ligands and the likely Ni spin state, while the Ni–Fe distance will affect the geometry of any hydride bridge. However, there is not complete agreement between the Ni–Fe site structures derived from X-ray diffraction, EXAFS analyses, and theoretical calculations.

Crystallographic and DFT predictions for Ni–S distances in as-isolated hydrogenase range from 2.20 to 2.69 Å (Table 1). For example, in the crystal structure of the oxidized *D. gigas* enzyme [7,26], the four Ni–S interactions can be divided into two pairs with average Ni–S distances of 2.2 and 2.6 Å. In the oxidized *D. vulgaris* Miyazaki structure, the bridging Ni–S distances are shorter (~2.38 Å), and the average Ni–S_{cys} bond length is 2.33 Å [8]. Both of these average crystallographic Ni–S distances, as well as the DFT prediction of 2.47 Å, are significantly longer than the 2.2 Å average that is reported in early EXAFS papers [20,21]. This trend persists for the reduced structures of the *D. vulgaris* [11] and *D. baculatum* [10] enzymes, where the crystallographic and DFT predictions remain longer than the EXAFS value of 2.19 Å (Table 1).

We have recently used L-edge X-ray absorption spectroscopy to probe the electronic structure of the Ni sites in a variety of hydrogenase samples [27]. The results were consistent with a covalent Ni(III) species for as-isolated hydrogenase, but the reduced forms of hydrogenase all appeared to contain high-spin Ni(II). The latter assignment is inconsistent with results from UV–visible MCD [28,29], parallel mode EPR [30], and saturation magnetization [31] methods, and these states have often been assigned as low-spin Ni(II) [12,24,29–32]. The ~2.2 Å average Ni–S distance found by EXAFS for H_2 reduced *D. gigas* hydrogenase [21] also presents a problem for the high-spin hypothesis, since this is a reasonable bond length for low-spin four-coordinate Ni-thiolate complexes. Churchill et al. found that the Ni–S distance fell in the range of 2.10–2.24 Å in Ni(II) complexes containing a diamagnetic square planar center [33]. Inspection of the Cambridge Structure Database [34] (CSD version 5.21) also reveals that all of the reported four-coordinate Ni(II) complexes with all sulfur ligands and an *average* Ni–S distance of less than 2.20 Å are in square planar or slightly distorted square planar geometry.

EXAFS spectra for many different hydrogenase preparations have been reported [18–22], and the average distances reported all tend to be ~2.2 Å. However, in all but a few cases, the maximum wave number for the EXAFS spectra reported to date was limited to 12.5 $Å^{-1}$. This is due to interference by the K-edge of trace amount of Cu, either in the samples or in the experimental apparatus. For example, Dole and coworkers reported the presence of trace amounts (~1%) of copper in their *D. gigas* hydrogenase preparations [30]. Since the spatial resolution in EXAFS is inversely related to the spectral range ($\Delta R = \pi/2\Delta k$), the limited range restricts the possibility of resolving individual Ni–S distances.

In this paper, we begin by presenting new EXAFS spectra for several Ni–Fe complexes to illustrate the issues of Ni–S/Ni–Fe shell resolution. We then report a method to extend EXAFS beyond an interfering absorption edge for a better special resolution. The method is tested using standard compounds with known structures. Finally, we use the model compound spectra to help interpret new

Table 1
Comparison of crystallographic, DFT, and EXAFS results

	EXAFS this work	XRD	XRD	DFT [a] [25]		DFT[a] [56]	DFT[a] [52]	DFT[a] [57]
As isolated	*D.g.*	*D.g.* [7]	*D.v.* [8]	S=1/2	S=3/2			
Ni–S average	2.27	2.45	2.33	2.46	2.48	2.51	2.44	2.36
Ni–Fe	N/A	2.9	2.55	2.89	2.99	2.94	2.96	2.82
Ni–O	1.91	1.7	2.16 (Ni–S)	1.86	1.93	1.86	1.84	1.86
Ni–S_t	2.18	2.2	2.22	2.32	2.38	2.48	2.40	2.29
Ni–S_t	2.18	2.3	2.33	2.33	2.33	2.44	2.44	2.37
Ni–S_b	2.35	2.6	2.37	2.50	2.46	2.47	2.41	2.35
Ni–S_b	2.35	2.6	2.38	2.69	2.76	2.63	2.49	2.41
H_2 reduced	*D.g.*	*D.b.* [10]	*D.v.* [11]	S=1	S=0		N/A	N/A
Ni–S average	2.34	2.35	2.33	2.52	2.60	2.44		
Ni–Fe	2.54	2.5	2.59	2.63	2.68	2.67		
Ni–O	2.03	None	None	None	None	None		
Ni–H	N/A	N/A	N/A	1.78	1.61	1.52		
Ni–S_t	2.21	2.2	2.24	2.34	2.35	2.39		
Ni–S_t	2.21	2.2	2.32	2.47	2.50	2.33		
Ni–S_b	2.47	2.5 (Ni–Se)	2.33	2.52	2.76	2.46		
Ni–S_b	2.47	2.5	2.43	2.74	2.78	2.58		

XRD, X-ray diffraction; DFT, Density Function Theory; *D.g., D. gigas; D.b., D. baculatum*; *D.v.=D. vulgaris*; S_t, terminal S; S_b, bridging S; in the EXAFS column, we assume that the long Ni–S is Ni–S_b.

[a] In the DFT calculations, 'as-isolated' and 'H_2 reduced' are form A and form R, respectively.

range-extended Ni EXAFS data for as-isolated and H_2 reduced *D. gigas* hydrogenase.

2. Experimental

2.1. Preparation of protein samples

D. gigas cultures were grown on a sulfate-lactate medium [35]. The H_2ase from these cultures was purified by ion-exchange chromatography as previously described [36,37]. Before the EXAFS measurements, the specific activity of the as-isolated samples, as measured by the hydrogen evolution method of Peck and Gest [38], was 450±50 units. One unit is defined as 1 μmol H_2 evolved per min per mg protein. The H_2 reduced sample had a specific activity of 470±30 units.

2.2. Enzyme film preparation

To achieve the highest possible Ni concentration, the H_2ase samples were prepared as partially dehydrated films. The purified *D. gigas* in phosphate buffer pH 7.8 was first degassed and kept under a purge of nitrogen gas for 30 min. A sheet of Kapton was placed in an anaerobic glass container that was kept under a constant purge of oxygen-free dry nitrogen gas. The protein solution was then layered onto the Kapton surface using a gas-tight syringe and allowed to partially dry into a film. Several layers of protein films were combined and mounted on the sample holder for EXAFS measurement. The total amount of protein in each sample was about 7–8 mg. After the X-ray measurements, both redissolved films showed a ~10% decrease in activity.

2.3. Preparation of model compounds

The binuclear complex [{Fe(NS_3)$(CO)_2$-S,S′}Ni-Cl(dppe)] [39] and the trinuclear complex [Ni{Fe(NS_3)(CO)-S,S′}$_2$] [40] were prepared in the Evans laboratory according to the cited literature procedures. Ni(II)$FeS_6P_2NO_2C_{54}H_{68}$[(n-Bu)$_4$N] was prepared in the Millar/Koch laboratory [41]. Ni[$(S_2C_2)Ph_2]_2$ was synthesized in the Stiefel laboratory according to published procedures [42]. Ni(aminothiophenolate)$_2$ was prepared in the Eichhorn laboratory [43]. CuF_2 and $CuCl_2$ were purchased from Aldrich. Model compounds were ground to a fine powder and diluted with boron nitride before loading into XAS (X-ray Absorption Spectroscopy) cells.

2.4. XAFS measurements

The Ni K-edge spectra were recorded at beamline 7-3 at the Stanford Synchrotron Radiation Laboratory (SSRL). Si(220) monochromator crystals were used with 2-mm slits for EXAFS scans and 1-mm slits for the XANES spectra. The energy was calibrated using a Ni foil as an internal standard in a three-ion chamber geometry, and the energy scale was calibrated using 8331.6 eV as the first inflection point of the Ni foil spectrum. All ion chambers were filled with N_2. Harmonic rejection was accomplished by detuning the second monochromator crystal to 50% of maximum possible flux. During all X-ray measurements, the samples were maintained at ca. 15 K using an Oxford Instruments CF1208 helium flow cryostat. To reduce radiation damage, the enzyme samples were moved to a different position after every fourth scan. The energy of Ni K-edge of the enzyme was monitored on sequential scans to confirm the stability of the enzyme in the X-ray beam.

Spectra were recorded from 8250 to 9400 eV in 30-min scans (12–18 scans per sample). The fluorescence data were collected using a Canberra 13-element Ge detector [25] and Canberra 2026 amplifiers using 0.125 μs shaping times. Single channel analyzers were used to set electronic windows on Ni Kα and Cu Kα fluorescence. The average Ni signal count rate at each individual detector element was ~6000 cps, while the total count rates were on the order of 100 000 cps.

2.5. XAFS data analysis

The EXAFS oscillations were extracted from the averaged spectra using the EXAFSPAK analysis software (courtesy of G.N. George), using 8350 eV as an initial E_0 for defining the photoelectron wave vector. The resultant EXAFS data were weighted by k^3 and Fourier-transformed over the region $k = 1$–16.5 Å^{-1}. Least-squares fits of the EXAFS data were carried out using Fourier-filtered data, using the following approximate formula to optimize the structural parameters N_b, R_{ab} and $\sigma_{ab}{}^2$:

$$\chi(k) = S_0^2(k)\sum_b \frac{N_b}{kR_{ab}^2}|f_b(k)|e^{-2\sigma_{ab}^2k^2}e^{-2R_{ab}/\lambda(k)} \times \sin(2kR_{ab} + \phi_{ab}(k))$$

In this equation, N_b is the number of backscatterers in the bth backscattering shell at distance R_{ab} from the X-ray absorber, $f_b(k)$ and $\phi_{ab}(k)$ are the backscattering amplitude and total phase-shift of the absorber–scatterer pairs, respectively, $\sigma_{ab}{}^2$ is the mean square deviation of R_{ab}, and $\lambda(k)$ represents the mean free path of the ejected photoelectron. $S_0^2(k)$ is an amplitude reduction factor that accounts for multiple electron excitations. The functions $f_b(k)$, $\phi_{ab}(k)$ and $\lambda(k)$ were calculated using the program FEFF 5.01 [44]. Values for ΔE_0 (the shift of E_0 from the initial value) for Ni–S (−6 eV) and Ni–Fe (−10 eV) interactions were determined from fits for Ni[$(S_2C_2)Ph_2$], and [Ni{Fe(NS_3)(CO)-S,S′}$_2$] model compounds, while a ΔE_0 of −9.2 eV was used for Ni–O components [45]. These ΔE_0 values were fixed during subsequent optimizations. The goodness of fit was determined by $F = \Sigma(\chi_{calc} - \chi_{obs})^2k^6$.

3. Results

3.1. Model compound and hydrogenase edges

To calibrate and check the parameters used in the EXAFS analysis, we recorded the spectra of several model compounds with Ni–Fe distances ranging from 2.5 to 3.3 Å. The K absorption edges for these models are shown in Fig. 1. The spectra clearly show the effects of different Ni geometries. The trinuclear complex [Ni{Fe(NS_3)(CO)-S,S′}$_2$] has a peak at ~8331 eV; this is a 1s→3d transition that is enhanced by p-d mixing in the tetrahedral Ni geometry [46]. In contrast, the binuclear complex [{Fe(NS_3)$(CO)_2$-S,S′}NiCl(dppe) has a sharp peak at ~8335 eV; this is a 1s→4p_z transition that is best resolved in square planar geometries [46]. The five-coordinate Ni(II)$FeS_6P_2NO_2C_{54}H_{68}$[(n-Bu)$_4$N] edge also has a clear 1s→3d transition and complex structure throughout the 1s→np region.

The K-edges for the as-isolated and H_2 reduced hydrogenase films are shown in Fig. 2. The as-isolated spectrum has an inflection point at 8342 eV and a 1s→3d transition at 8334 eV, with a normalized integrated intensity of 0.046 consistent with its five-coordinate structure [21,32]. The spectrum of the H_2 reduced sample shows a shift to lower energy compared to the as-isolated enzyme—the inflection point shifts lower by ca. 0.8 eV. The pre-edge intensity in H_2 reduced (0.036) is weaker than for as-isolated hydrogenase, suggesting a more centrosymmetric Ni geometry and/or fewer 3d vacancies upon reduction. This reduction in intensity has been seen before [21,22].

3.2. Ni–Fe model compound EXAFS

The model compound EXAFS data, Fourier transforms, and fits are presented in Fig. 3. The Fourier transform for the binuclear [{Fe(NS_3)$(CO)_2$-S,S′}NiCl(dppe) complex shows a clear Ni–Fe peak at 3.3 Å in the phase-shift-corrected transform. For the trinuclear model, with two Ni–Fe interactions and a 0.4 Å separation between Ni–Fe and Ni–S shells, again there are two well-resolved peaks for these Ni–S and Ni–Fe interactions. Thus, in favorable cases, Ni–Fe interactions can be seen between 2.6 and 3.3 Å. However, the transform for Ni(II)$FeS_6P_2NO_2C_{54}H_{68}$[(n-Bu)$_4$N] shows only a single broad peak—Ni–S at 2.26 Å and Ni–Fe components at 2.50 Å are not resolved. Despite these difficulties in interpretation of the Fourier transform, the Ni–S and Ni–Fe distances obtained by curve-fitting the *k*-space spectra for this model were, respectively within 0.05 Å and 0.02 Å of the X-ray diffraction values. For the other models, the accuracy was always 0.03 Å or better (Table 2). The difficulties associated with analyzing closely spaced Ni–S and Ni–Fe components have been discussed in detail by Scott and coworkers [21,22]. Similar problems occur with overlapping Cu–S and Cu–Cu components in Cu_A sites [47] and interfering Fe–S and Fe–Fe components in the fully reduced nitrogenase Fe protein [48].

Our goal in this work has been to achieve better spatial resolution from limited EXAFS data. Even if two shells with the same element are not resolved and have to be modeled by a single component, the interference between the two will result in an anomalously high σ value that

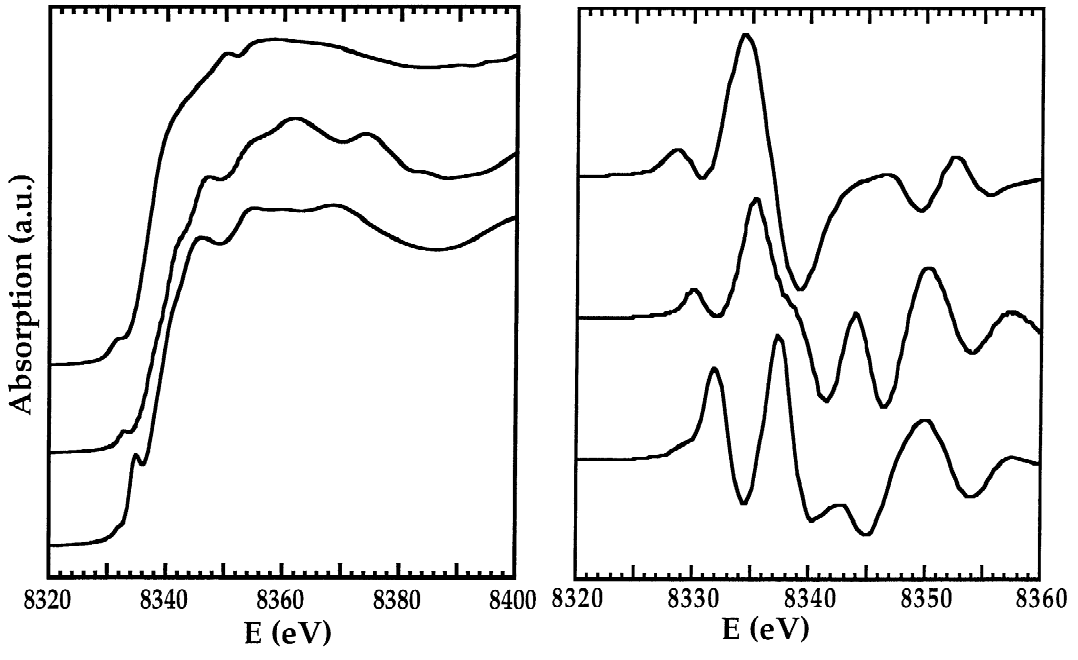

Fig. 1. (Left) Ni K-edge spectra for (top to bottom) [Ni{Fe(NS_3)(CO)-S,S′}$_2$], Ni(II)$FeS_6P_2NO_2C_{54}H_{68}$[(n-Bu)$_4$N], and [{Fe(NS_3)$(CO)_2$-S,S′}NiCl(dppe). (Right) Second derivative curves for the K-edge spectra reported in the left panel.

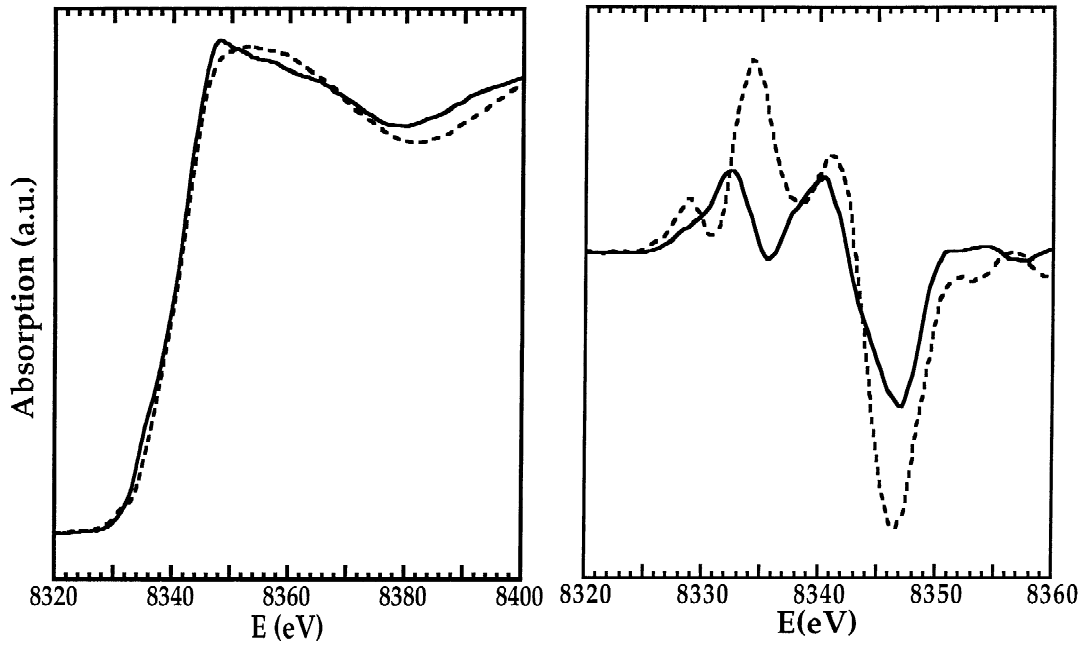

Fig. 2. (Left) Ni K-edge spectra for as-isolated (- - -) and H_2 reduced (———) hydrogenase films. (Right) Second derivative curves for the K-edge spectra reported in the left panel.

reflects both thermal motion and static disorder. Using data for compounds with homogeneous Ni–S distances, we therefore investigated the range of normal values for purely thermal disorder. Vibrational frequencies and force constants diminish with increasing bond length, hence this thermal disorder in bond lengths should increase with distance [49]. Using our own data as well as literature values [18], we have plotted the correlation between σ^2 and R in Fig. 4. We find that σ (σ^2) for a Ni–S bond ranges from 0.045 Å (0.002 Å^2) for the shortest Ni–S

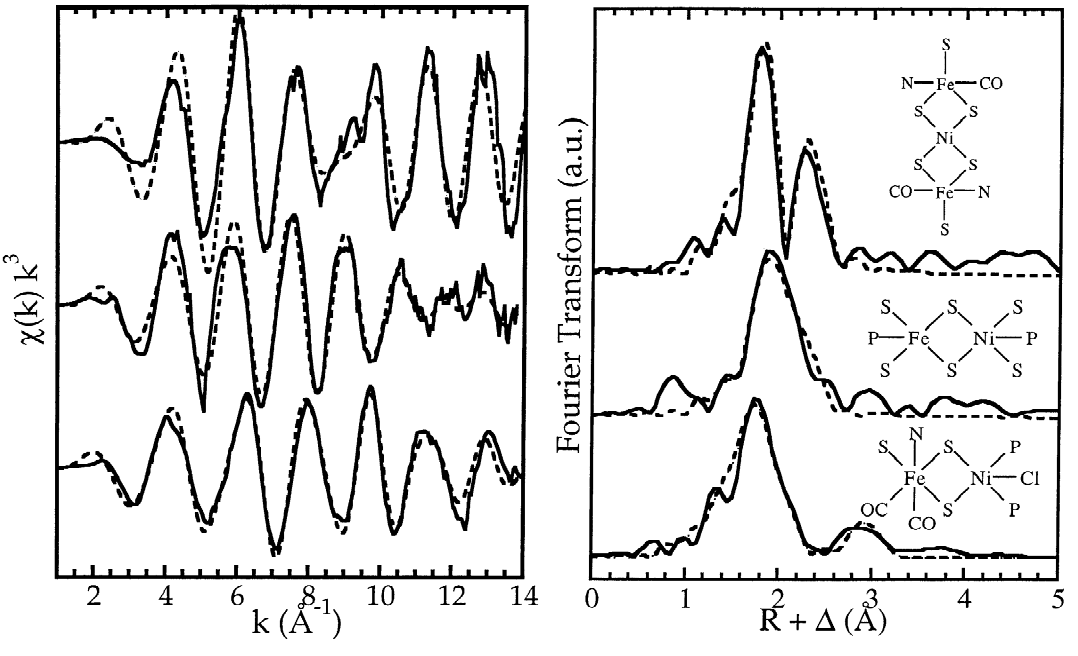

Fig. 3. (Left) EXAFS *k*-space spectra (———) and best fits (- - -) for (top to bottom) [Ni{Fe(NS_3)(CO)-S,S′}$_2$], Ni(II)$FeS_6P_2NO_2C_{54}H_{68}$[(n-Bu)$_4$N], and [{Fe(NS_3)$(CO)_2$-S,S′}NiCl(dppe). (Right) EXAFS Fourier transforms (———) and best fits (- - -) for compounds in the left panel. A schematic drawing of each compound is on the right-hand side of each transform.

Table 2
Ni–Fe model compound EXAFS results

Compound	*N*	*R* (Å)	σ^2 (10^{-3} Å^2)	*F*	Crystal data
[{Fe(NS_3)($CO)_2$-S,S′}NiCl(dppe)]	4S	2.18	6.3	675.3	1S 2.247
	4S 1Cl	2.19 2.48	6.5 4.5	522.4	1S 2.255 1P 2.164 1P 2.196
	4S 1Cl 1Fe	2.18 2.48 3.29	6.3 4.3 3.0	391.1	1Cl 2.508 1Fe 3.308
Ni(II)$FeS_6P_2NO_2$ $C_{54}H_{68}$[(n-Bu)$_4$N]	4S	2.33	6.7	629.1	1S 2.254
	4S 1P	2.36 2.23	4.4 1.0	499.0	1S 2.253 1S 2.257 1S 2.290
	4S 1P 1Fe	2.31 2.05 2.55	6.6 16.5 2.7	341.0	1P 2.107 1Fe 2.530
[Ni{Fe(NS_3)-(CO)S,S′}$_2$]	4S 2Fe	2.23 2.61	4.1 3.4	598.9	2S 2.229 2S 2.287 2Fe 2.637

bonds near 2.15 Å to 0.100 Å (0.010 Å^2) for bonds near 2.48 Å. Since σ^2 appears in the exponential of the Debye–Waller factor, these differences cause wide (orders of magnitude) variations in EXAFS amplitudes. The important point from this analysis is that *vibrational* contribution to σ (σ^2) for a Ni–S bond near 2.2 Å is expected to be $<$0.055 Å (0.003 Å^2). Disorder above that value is expected to arise from a *static* variation in Ni–S distances over two or more distinct Ni–S bonds.

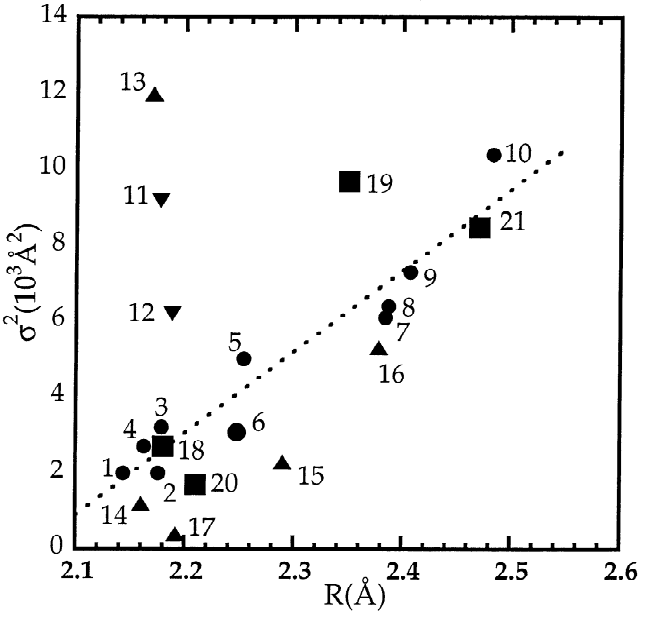

Fig. 4. The correlation between σ^2 and *R* for a variety of Ni–S bonds. The dotted line represents the linear fit of the model compounds data. Key: ●, Ni model compounds EXAFS data from literature [18]; ▼, *D. gigas* H_2ase EXAFS data from literature [21]; ▲, *C. vinosum* H_2ase EXAFS data from literature [22]; ■, EXAFS data of this work, 18,19: as-isolated (two Ni–S shells), 20,21: H_2 reduced (two Ni–S shells). The detailed numbering correspondence can be found in the supplementary material. (See the Elsevier website http://www.elsevier.com/homepage/saa.jib)

3.3. The 'range-extended' EXAFS procedure

Typical Ni EXAFS oscillations are less than a 1% modulation at 9000 eV (the Cu K-edge). Thus, even a trace amount of Cu will overwhelm the Ni EXAFS signal. To achieve a wider *k*-range and hence a better spatial resolution in the EXAFS analysis, we developed a procedure to subtract interfering Cu signals. There is no fundamental reason to doubt the subtraction procedure. However, the method involves subtraction of two large signals and analysis of a much smaller difference spectrum, and it is subject to artifacts if the subtraction is not done properly. In order to test our subtraction procedures, the spectra of two Ni compounds were analyzed before and after addition of trace amounts of Cu (Fig. 5). Specifically, CuF_2 and $CuCl_2$ were added to Ni[$(S_2C_2)Ph_2]_2$ and $NiS_2(NH_2)_2Ph_2$ samples, respectively to obtain approximately the same fractional Cu signal as observed in the protein spectra.

The key parameter in this subtraction procedure is the weight assigned to the Cu signal. This was estimated by visually determining the thresholds for scale factors that were clearly too large or too small, and then using the average of these two limiting factors. As shown in Fig. 5, the corrected EXAFS of the Cu-doped materials is very similar to the undoped Ni compound. There may be small artifacts in the vicinity of the Cu edge, but the Ni EXAFS signal is a long wavelength oscillation distributed over tens of eV, hence the Fourier transforms of undoped and corrected EXAFS are virtually identical.

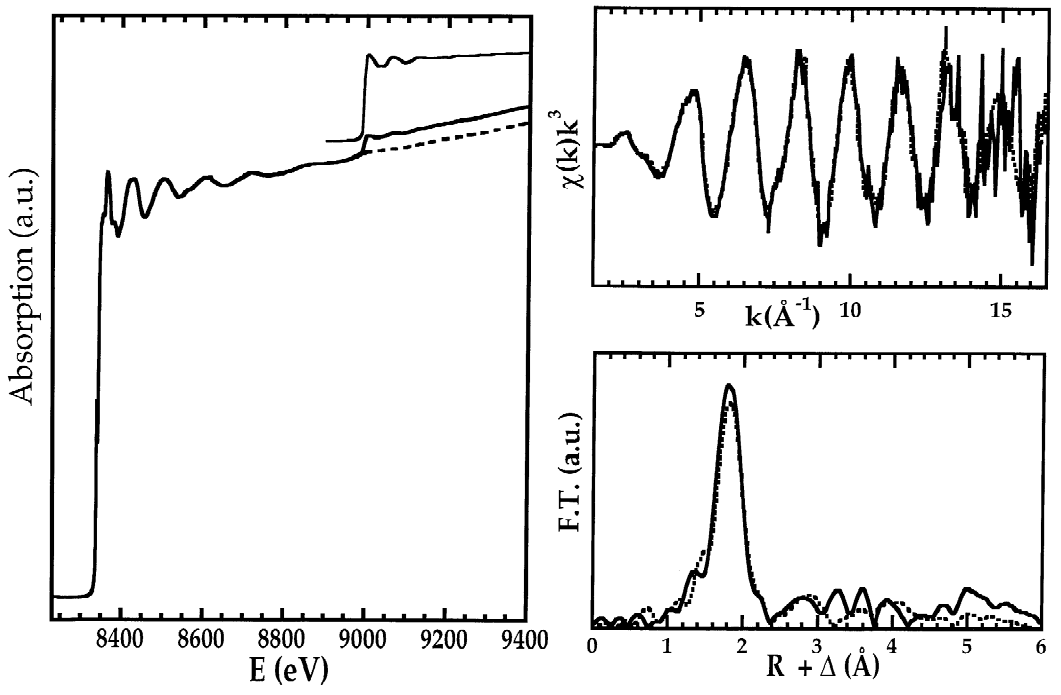

Fig. 5. (Left) The dual energy window subtraction procedure. Raw Ni spectrum for a Cu-doped sample of $Ni[(S_2C_2)Ph_2]_2$ (———); Cu spectrum for the same (———); and result of subtracting a scaled amount of the Cu spectrum from the raw Ni spectrum (- - -). (Right) Comparison of *k* space (top) and Fourier-transformed (bottom) EXAFS spectra for a $Ni[(S_2C_2)Ph_2]_2$ sample without Cu contamination (———) versus corrected spectra for a Cu-doped sample (- - -).

3.4. Hydrogenase EXAFS

Fig. 6 compares the conventional and the range extended EXAFS of *D. gigas* hydrogenase. Over the wider *k* range (1–16.5 $Å^{-1}$), the spectra exhibit features which are not seen on a range limited by Cu contamination ($k = 2$–12.5 $Å^{-1}$). The main peak in the as-isolated Fourier transform begins to show a splitting, while in the H_2 reduced transform, a longer distance peak emerges from the truncation ripple. Overall, the differences between as-isolated and H_2 reduced spectra are more pronounced on the wider range data, illustrating the significant structural change that occurs at the Ni site.

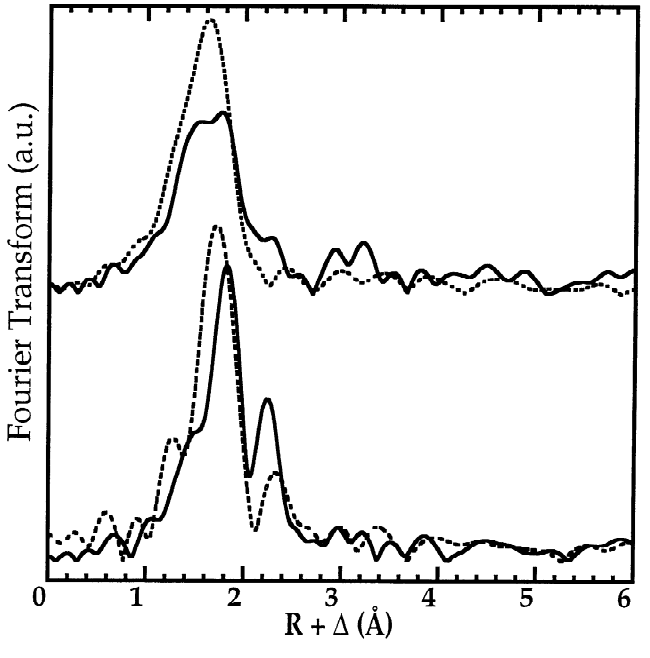

Fig. 6. Conventional (- - -) and range-extended (———) EXAFS Fourier transforms for (top) as-isolated and (bottom) H_2 reduced *D. gigas* H_2ase. Transform ranges were $\Delta k = 10.5$ and $\Delta k = 15.5$, respectively.

Fig. 7 shows simulations of the raw *k*-space and Fourier transformed EXAFS of both as-isolated and fully H_2 reduced enzymes, calculated after removal of the Cu signal. Relevant fits for the hydrogenase EXAFS spectra are summarized in Table 3. For the as-isolated sample, fitting the Ni EXAFS with a single S shell yields a 2.19 Å Ni–S distance, in agreement with previous studies. However, the σ value (0.095 Å) is very large compared to model compounds with homogenous Ni–S distances. The fit is improved by more than a factor of two using two sub-shells with two Ni–S at 2.17 Å and two Ni–S at 2.35 Å, and the individual σ values become more reasonable. We note that the X-ray crystal structure has a 0.3 Å split between the average bond lengths for terminal and bridging sulfur ligands [7,10].

Another dramatic improvement in fit quality is obtained by introducing a short Ni–O interaction—this is one proposal for the bridging ligand 'X'. As illustrated in the 'search profile' (Fig. 8), adding one Ni–O component at

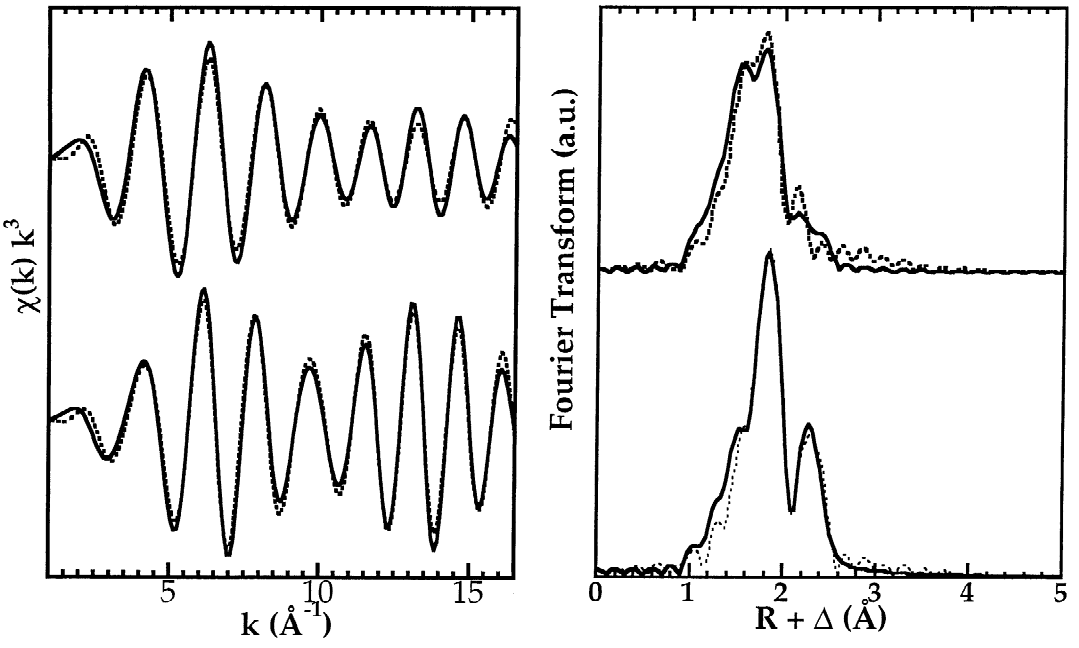

Fig. 7. (Left) Fourier-filtered (backtransform window = 1.0–2.8 Å) EXAFS *k*-space spectra (———) and best fits (- - -) for (top) as-isolated and (bottom) H_2 reduced *D. gigas* H_2ase. (Right) EXAFS Fourier transforms for the spectra (———) and the best fits (- - -) reported in the left panel.

1.91 Å improves the fit more than twofold. Our distance is in agreement with other EXAFS work.

We were less successful in identifying the Ni–Fe distance in as-isolated hydrogenase. Since the crystal structure shows a Ni–Fe distance at ca. 2.9 Å [7,26], we investigated the effects of including such a Ni–Fe interaction. Adding one Fe at 2.78 Å improved the fit by 20%, but the σ value (0.11 Å) was very large. A better fit is obtained by adding 0.5 Fe at 2.77 Å, and this leads to a fit with a physically reasonable σ (0.08 Å). However, replacing this Fe shell by 0.5 S at 2.59 Å leads to the same quality of fit. At this time, we cannot unambiguously identify the Ni–Fe distance; this may be due to: (a) interference between Ni–Fe and long Ni–S components (as discussed in the model compound section), (b) structural disorder in the samples, or (c) a combination of both effects.

Table 3
Range-extended hydrogenase EXAFS analysis

Form	Fit	*N*	*R* (Å)	σ^2 (10^{-3} Å^2)	*F*
As isolated	1a	4 S	2.19(2)	9.2	258.3
	2a	2 S	2.17(2)	3.1	113.4
		2 S	2.33(5)	11.1	
	3a	1 O	1.91(2)	2.5	40.7
		2 S	2.18(2)	2.7	
		2 S	2.35(5)	9.7	
H_2-reduced	1A	4 S	2.22(2)	5.6	605.7
	2A	2 S	2.20(2)	0.7	167.9
		2 S	2.35(5)	5.2	
	3A	2 S	2.21(2)	1.2	76.1
		2 S	2.43(5)	11.4	
		1 Fe	2.52(5)	2.6	
	3B	2 S	2.21(2)	1.0	91.9
		1 S	2.38(2)	1.8	
		1 S	2.66(5)	1.8	
	4A	1 O	2.03(2)	1.4	24.5
		2 S	2.21(2)	1.7	
		2 S	2.47(5)	8.5	
		1 Fe	2.54(5)	1.8	

For the H_2 reduced spectrum, the fit is improved threefold by splitting the Ni–S shell into two sub-shells, now with 2 S at 2.20 Å and 2 S at 2.35 Å. Adding a third shell of one Fe at 2.52 Å (the long Ni–S distance changes to 2.43 Å accordingly) also improves the fit by another factor of two. This is in good agreement with crystallographic observations of a shorter Ni–Fe distance in the H_2 reduced samples. For all of these fits, the σ values become much more reasonable than the single-shell analysis (Fig. 4: number 20 and 21). In an alternate fit, the Ni–Fe component can be replaced by a long Ni–S at 2.66 Å. However, this fit requires an unusually small σ for such a long Ni–S distance, and is most likely an artifact due to the π difference in Ni–S and Ni–Fe phase shifts [21]. We therefore prefer the former fit, which also agrees better with the crystal structure.

The contour plot gives an indication for the correlation between the selected parameters [50]. Since we observe that the long Ni–S distance goes to 2.43 Å by adding the third shell of Fe at 2.52 Å (fit 3A, Table 3), the correlation between the long Ni–S and Ni–Fe is analyzed by contour plot (Fig. 8, right). The contour minimum occurs where

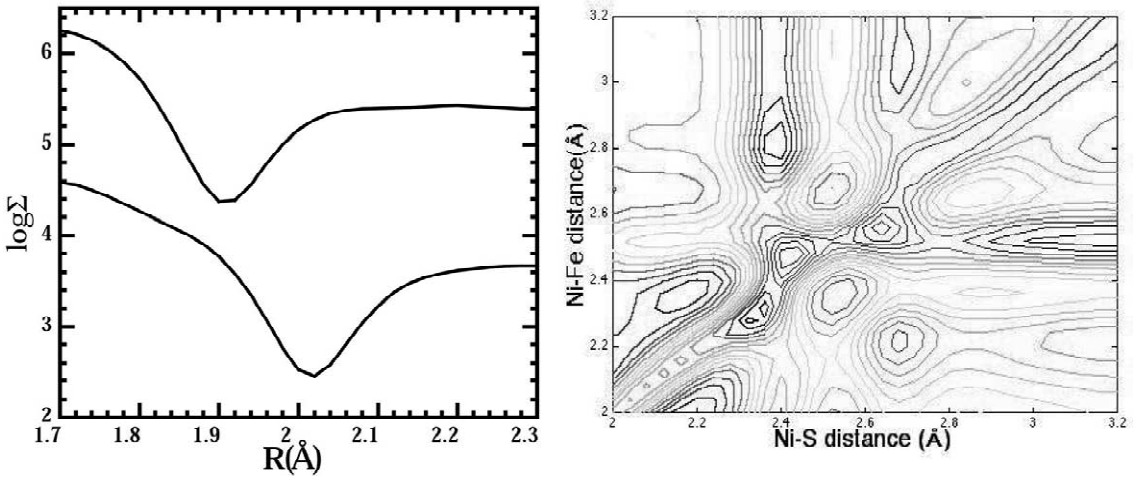

Fig. 8. (Left) Search profile for Ni–O component in (top) as-isolated and (bottom) H_2 reduced *D. gigas* H_2ase. Searches were performed from 1.7 to 2.3 Å. Σ is defined as $[\Sigma k^6(\chi_{calc} - \chi_{obs})^2/n]^{1/2}$. (Right) Contour plot illustrating the correlation between Ni–Fe and the long Ni–S distance in fits of H_2 reduced H_2ase. Search was carried out from 2.0 to 3.2 Å for both Ni–S and Ni–Fe components. The Σ minimum is at 2.43 and 2.52 Å for long Ni–S and Ni–Fe, respectively.

Ni–S is at 2.43 Å and Ni–Fe at 2.52 Å. Judging from the tilt of the principal axis of the ellipses, there is not strong correlation between the two parameters.

For completeness, we investigated whether the short Ni–O component found in as-isolated, often assigned as a bridging hydroxide, disappears in the H_2 reduced spectrum. To our surprise, addition of one Ni–O component at ca. 2.03 Å increases the goodness of fit criterion by a factor of three (fit 4A, Table 3). This could indicate the presence of a water molecule as a Ni ligand. However, there is no evidence for this in the crystal structures. A more exotic possibility is that we are seeing evidence for Ni–H interactions—some of the DFT calculations propose two hydrides as ligands to Ni in H_2 reduced form [10,25,51–53]. A more mundane interpretation is that ~15% of the Ni in the sample has fallen out of the active site and remains as hexaaquo Ni(II). We are planning experiments to distinguish these possibilities.

From the fits in Table 3, we see that the average Ni–S bond length in the H_2 reduced enzyme is most likely not the 2.22 Å value given by a single shell analysis, but anywhere from a minimum of 2.27 Å to beyond 2.3 Å, depending on the model employed. As illustrated in Fig. 9, the Ni–S bond length can in certain cases be a good indicator of the Ni(II) spin state. Average Ni–S distances range from 2.10 to 2.24 Å for approximately square planar complexes, compared to 2.27 to 2.31 Å for tetrahedral complexes. An average of 2.29 Å is found for five-coordinate Ni(II) complexes compared to 2.43 Å in six-coordinate complexes. If the H_2 reduced Ni–S distance were indeed 2.22 Å, that would be a strong indication of low-spin Ni(II), but values in the 2.34 Å range are much more ambiguous.

Recent DFT calculations by Fan and Hall for H_2 reduced hydrogenase found that the optimized structures for a unconstrained Ni(II) geometries yielded nearly equivalent energies for high-spin and low-spin Ni(II) sites [54]. However, they also found that if the Ni–S bonds were constrained to a geometry similar to the crystallographic results, the high-spin state had the lowest energy by nearly 20.0 kcal/mol [54]. This raises the interesting possibility that the Ni spin state is controlled by the position of the protein ligands, making H_2 reduced hydrogenase Ni a new candidate for a bioinorganic entatic state.

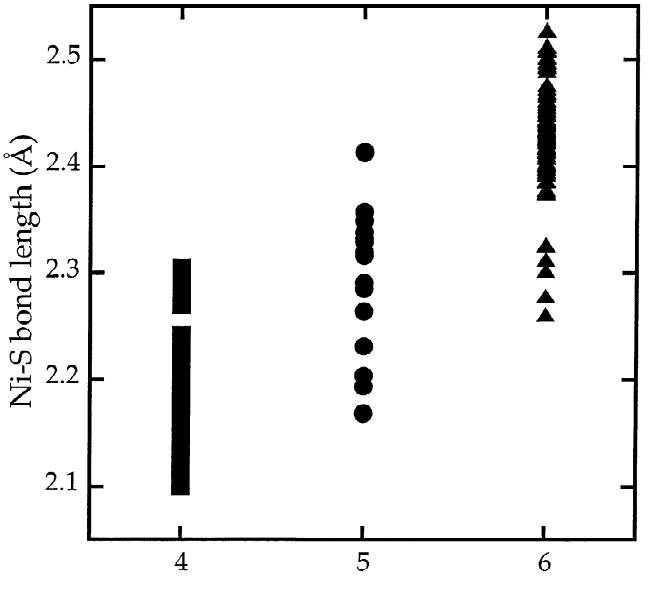

Fig. 9. The average Ni–S distances for four- (■), five- (●) or six- (▲) coordinated Ni compounds. The search was carried out in the Cambridge Structure Database (CSD version 5.12).

This potential mechanism for protein control of the Ni spin state in enzymes was noted years ago [55].

4. Summary

We have developed a new procedure, 'range-extended EXAFS', for recording and analyzing EXAFS spectra past the edges of interfering elements. We have applied this technique to record hydrogenase Ni EXAFS spectra past the interference from adventitious Cu. The improved resolution from using the range-extended technique helps reveal that the Ni–S distances at the active site are not homogeneous in both as-isolated and H_2 reduced hydrogenase (in agreement with both crystallography and DFT calculations). When the Ni–S interactions are broken into two components, the average distance deduced from EXAFS is significantly longer than in single shell analyses. Inferences about the Ni spin state in H_2 reduced hydrogenase, based on the Ni–S bond length, need to take this longer average bond length into account.

Acknowledgements

We would like to thank Drs Edward Stiefel and Kun Wang for the sample of $Ni[(S_2C_2)Ph_2]_2$. This work was supported by the National Institutes of Health Grants GM-44380 (S.P.C.), and the DOE Office of Biological and Environmental Research. The Biotechnology and Biological Sciences Research Council, UK is also acknowledged for financial support (D.J.E. and M.C.S.). SSRL is supported by the Department of Energy, Office of Basic Energy Sciences.

References

[1] J. Quakernaat, Int. J. Hydrogen Energy 20 (1995) 485–492.
[2] P.C. Novelli, P.M. Lang, K.A. Masarie, D.F. Hurst, D.R. Meyers, J.W. Elkins, J. Geophys. Res. Atmos. 104 (1999) 30427–30444.
[3] D. Morgan, F. Sissine, Congressional Research Service Report for Congress—Hydrogen: Technology and Policy, 1995, http://www.cnie.org/nle/eng-4.html
[4] J.O.M. Bockris, Int. J. Hydrogen Energy 24 (1999) 1–15.
[5] M.W.W. Adams, E.I. Stiefel, Curr. Opin. Chem. Biol. 4 (2000) 214–220.
[6] J.C. Fontecilla-Camps, M. Frey, E. Garcin, C. Hatchikian, Y. Montet, C. Piras, X. Vernede, A. Volbeda, Biochemie 79 (1997) 661–666.
[7] A. Volbeda, E. Garcin, C. Piras, A.L. de Lacey, V.M. Fernandez, E.C. Hatchikian, M. Frey, J.C. Fontecilla-Camps, J. Am. Chem. Soc. 118 (1996) 12989–12996.
[8] Y. Higuchi, T. Yagi, N. Yasuoka, Structure 5 (1997) 1671–1680.
[9] P.M. Matias, C.M. Soares, L.M. Saraiva, R. Coelho, J. Morais, J. Le Gall, M.A. Carrondo, J. Biol. Inorg. Chem. 6 (2001) 63–81.
[10] E. Garcin, X. Vernede, E.C. Hatchikian, A. Volbeda, M. Frey, J.C. Fonecilla-Camps, Struct. Folding Des. 5 (1999) 557–566.
[11] Y. Higuchi, H. Ogata, K. Miki, N. Yasuoka, T. Yagi, Struct. Folding Des. 7 (1999) 549–556.
[12] K.A. Bagley, C.J. Vangarderen, M. Chen, E.C. Duin, S.P.J. Albracht, W.H. Woodruff, Biochemistry 33 (1994) 9229–9236.
[13] K.A. Bagley, E.C. Duin, W. Roseboom, S.P.J. Albracht, W.H. Woodruff, Biochemistry 34 (1995) 5527–5535.
[14] A.L. de Lacey, E.C. Hatchikian, A. Volbeda, M. Frey, J.C. Fontecilla-Camps, V.M. Fernandez, J. Am. Chem. Soc. 119 (1997) 7181–7189.
[15] R. Cammack, D. Patil, R. Aguirre, E.C. Hatchikian, FEBS Lett. 142 (1982) 289–292.
[16] S.P.J. Albracht, M.I. Kalkman, E.C. Slater, Biochim. Biophys. Acta 724 (1983) 309–316.
[17] M. Asso, B. Guigliarelli, T. Yagi, P. Bertand, Biochim. Biophys. Acta Bioenerg. 1122 (1991) 50–56.
[18] M.J. Maroney, G.J. Colpas, C. Bagyinka, N. Baidya, P.K. Mascharak, J. Am. Chem. Soc. 113 (1991) 3962–3972.
[19] J.P. Whitehead, G.J. Colpas, C. Bagyinka, M.J. Maroney, J. Am. Chem. Soc. 113 (1991) 6288–6289.
[20] J.P. Whitehead, R.J. Gurbiel, C. Bagyinka, B.M. Hoffman, M.J. Maroney, J. Am. Chem. Soc. 115 (1993) 5629–5635.
[21] Z.J. Gu, J. Dong, C.B. Allan, S.B. Choudhury, R. Franco, J.J.G. Moura, J. Legall, A.E. Przybyla, W. Roseboom, S.P.J. Albracht, M.J. Axley, R.A. Scott, M.J. Maroney, J. Am. Chem. Soc. 118 (1996) 11155–11165.
[22] G. Davidson, S.B. Choudhury, Z. Gu, K. Bose, W. Roseboom, S.P.J. Albracht, M.J. Maroney, Biochemistry 39 (2000) 7468–7479.
[23] M.J. Maroney, P.A. Bryngelson, J. Biol. Inorg. Chem. 6 (2001) 453–459.
[24] S. Niu, L.M. Thomson, M.B. Hall, J. Am. Chem. Soc. 121 (1999) 4000–4007.
[25] P. Amara, A. Volbeda, J.C. Fontecilla-Camps, M.J. Field, J. Am. Chem. Soc. 121 (1999) 4468–4477.
[26] A. Volbeda, M.H. Charon, C. Piras, E.C. Hatchikian, M. Frey, J.C. Fontecilla-Camps, Nature 373 (1995) 580–587.
[27] H. Wang, C.Y. Ralston, D.S. Patil, R.M. Jones, W. Gu, M. Verhagen, M.W.W. Adams, P. Ge, C. Riordan, C.A. Marganian, P. Mascharak, J. Kovacs, C.G. Miller, T.J. Collins, S. Brooker, P.D. Croucher, K. Wang, E.I. Stiefel, S.P. Cramer, J. Am. Chem. Soc. 122 (2000) 10544–10552.
[28] M. Cheesman, Ph.D. Thesis, University of East Anglia, 1989.
[29] A.T. Kowal, I.C. Zambrano, I. Moura, J.J.G. Moura, J. LeGall, M.K. Johnson, Inorg. Chem. 27 (1988) 1162–1166.
[30] F. Dole, A. Fournel, V. Magro, E.C. Hatchikian, P. Bertrand, B. Guigliarelli, Biochemistry 36 (1997) 7847–7854.
[31] C.P. Wang, R. Franco, J.J.G. Moura, I. Moura, E.P. Day, J. Biol. Chem. 267 (1992) 7378–7380.
[32] C. Bagyinka, J.P. Whitehead, M.J. Maroney, J. Am. Chem. Soc. 115 (1993) 3576–3585.
[33] M.R. Churchill, J. Cooke, J.P. Fennessey, J. Wormald, Inorg. Chem. 10 (1971) 1031–1035.
[34] F.H. Allen, J.E. Davies, J.J. Galloy, O. Johnson, O. Kennard, C.F. Macrae, E.M. Mitchell, G.F. Mitchell, J.M. Smith, D.G. Watson, J. Chem. Inform. Comput. Sci. 31 (1991) 187–204.
[35] J. LeGall, N. Forget, Methods Enzymol. 53 (1974) 613.
[36] S.H. He, M. Teixeira, J. LeGall, D.S. Patil, I. Moura, J.J.G. Moura, D.V. DerVartanian, B.H. Huynh, H.D. Peck Jr., J. Biol. Chem. 264 (1989) 2678–2682.
[37] D.S. Patil, Methods Enzymol. 243 (1994) 68–94.
[38] H.D. Peck Jr., H. Gest, J. Bacteriol. 71 (1965) 70–73.
[39] S.C. Davies, D.J. Evans, D.L. Hughes, S. Longhurst, J.R. Sanders, Chem. Commun. (1999) 1935–1936.
[40] M.C. Smith, S. Longhurst, J.E. Barclay, S.P. Cramer, S.C. Davies, D.L. Hughes, W.-W. Gu, D.J. Evans, J. Chem. Soc. Dalton Trans. (2001) 1387–1388.
[41] M. Millar, S.A. Koch, personal commun.: Ni–Fe model compound, 1997.

[42] J.D. Saftain, M.R. Truter, J. Chem. Soc. (1967) 1264.
[43] E.J. Olszewski, M.J. Albinak, J. Inorg. Nucl. Chem. 27 (1965) 1431–1433.
[44] J.J. Rehr, J. Mustre De Leon, S.I. Zabinsky, R.C. Albers, J. Am. Chem. Soc. 113 (1991).
[45] I.J. Pickering, G.N. George, J.T. Lewandowski, A.J. Jacobson, J. Am. Chem. Soc. 115 (1993) 4137–4144.
[46] M.K. Eidsness, R.J. Sullivan, R.J. Scott, in: J.R. LancasterJr. (Ed.), The Bioinorganic Chemistry of Nickel, Electronic and Molecular Structure of Biological Nickel as Studied by X-Ray Absorption Spectroscopy, VCH Publishers, New York, 1988, pp. 73–91.
[47] N.J. Blackburn, M.E. Barr, W.H. Woodruff, J. Vanderooost, S. Devries, Biochemistry 33 (1994) 10401–10407.
[48] K.B. Musgrave, H.C. Angove, B.K. Burgess, B. Hedman, K.O. Hodgson, J. Am. Chem. Soc. 120 (1998) 5325–5326.
[49] S.P. Cramer, K.V. Rajagopalan, R. Wahl, J. Am. Chem. Soc. 103 (1981) 7721–7727.
[50] H.H. Zhang, A. Filipponi, A. Dicicco, S.C. Lee, M.J. Scott, R.H. Holm, B. Hedman, K.O. Hodgson, Inorg. Chem. 35 (1996) 4819–4828.
[51] H.-J. Fan, M.B. Hall, J. Biol. Inorg. Chem. 6 (2001) 467–473.
[52] M. Stein, W. Lubitz, Phys. Chem. Chem. Phys. 3 (2001) 2668–2675.
[53] M. Stein, E. van Lenthe, E.J. Baerends, W. Lubitz, J. Am. Chem. Soc. 123 (2001) 5839–5840.
[54] H.J. Fan, M.B. Hall, J. Am. Chem. Soc. 124 (2002) 394–395.
[55] C.L. Coyle, E.I. Stiefel, in: J.R. LancasterJr. (Ed.), The Bioinorganic Chemistry of Nickel, The Coordination Chemistry of Nickel: An Introductory Survey, VCH Publishers, New York, 1988, pp. 1–28.
[56] L. De Gioia, P. Fantucci, B. Guigliarelli, P. Bertrand, Inorg. Chem. 38 (1999) 2658–2662.
[57] S.H. Li, M.B. Hall, Inorg. Chem. 40 (2001) 18–24.